Proceedings of the 1998 IEEE
International Conference on Robotics & Automation
Leuven, Belgium • May 1998

Perception of an Indoor Robot Workspace by Using CTFM Sonar Imaging

Zafiris Politis and Penny Probert

{zpol,pjp}@robots.ox.ac.uk

Robotics Research Group
Department of Engineering Science
University of Oxford
Parks Road, Oxford OX 3PJ, UK

Abstract– *Ultrasonic sensors have been widely used as time-of-flight range finding systems in mobile robots. Different variations of this scheme lead to robust identification of simple reflector types, like walls, corners and edges. In this paper an alternative approach is attempted, able not only to locate and identify simple reflectors, but to detect and recognize more complicated objects. A more sophisticated sensor, the CTFM sonar, produces an image which corresponds to a range map. The image provides information about the location and type of the reflector. A reflectivity model for planes, corners, and edges is presented and compared with some experimental results. A method to distinguish well structured reflectors from complex objects is then described and the application of the system in a room mapping task is demonstrated.*

Keywords– *Acoustics, CTFM sonar, machine perception, map building, mobile robots.*

1 Introduction

Sonar is well established as a sensor for mapping the robot workspace. Leonard and Durrant-Whyte [1] show how a very simple pulsed sensor which measured the distance only to the nearest object can discriminate between planes and corners through spatial integration of readings, in dense angular scans. Clearly this type of sensor throws away a lot of information through ignoring all returns except the first. Barshan and Kuc [2], and Peremans [3] retain this information through examining a complete time history of the reflection, rather than simply just the first return, to examine the impulse response of different types of reflectors and hence to provide discrimination by taking a scan using two T/R pairs and a single shot using a tri-aural system respectively. However noise is a major difficulty in pulsed systems.

The sensor we investigate here has two advantages over these systems. First it is swept in frequency and hence inherently offers a better resolution for discriminating between adjacent features through exploiting a wider bandwidth. Chirped pulsed sensors can also, of course, exploit this advantage. However the pseudo continuous wave nature of the sensor offers advantages in signal to noise ratio which the pulsed sensor cannot match, since greater energy is emitted into the environment. In this paper we show that this allows us to discriminate planes, corners, and edges by taking a scan using just one T/R pair.

In section 2 we present a brief introduction to the system, together with a model for its application to simple reflectors, i.e. planes, corners, and edges. Section 3 demonstrates the application of the model for real data and introduces a method to discriminate between these features. In section 4 we describe methods of extracting features such as these from more complex data, and in section 5 we demonstrate the application of the sensor in map building.

2 The general concept

In this work a simple CTFM sonar device is configured with one transmitter and one receiver. A continuous transmission frequency modulated system is used, operating over a frequency range of f_l (45kHz) to f_h (90kHz), using the saw-tooth frequency pattern of figure 1. Assuming that the frequency bandwidth is

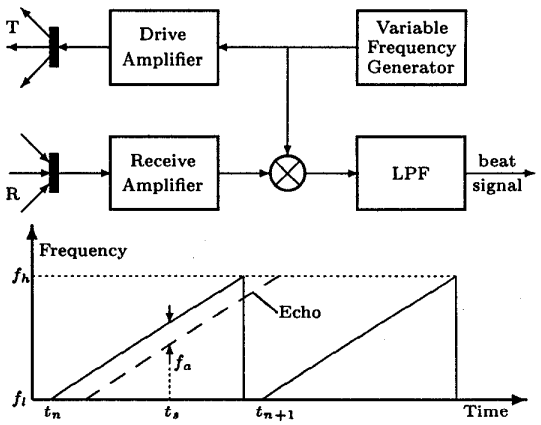

Figure 1: The used CTFM sonar and the frequency pattern of the transmitter.

not increased by the saw-tooth modulation, the transmitted signal s_T is of the form [5]

$$s_T(t) = A\mathrm{Re}\left\{e^{2\pi j(f_l t_s + m t_s^2)}\right\}, \quad t_n \le t < t_{n+1} \quad (1)$$

where $t_s = t - t_n$ is the time during a sweep cycle, i.e. $0 \le t_s \le T_s$, $T_s \backsimeq t_{n+1} - t_n$ (184ms) is the sweep period, and m is a constant ($m = \frac{f_h - f_l}{T_s}$).

Mixing the returning signal with the signal currently being transmitted, and filtering out high frequencies, produces a difference signal containing only one frequency f_a, which corresponds to the range of the object from which reflection has occurred.

The signal returned from a number of elementary (compared to the object size) surfaces irregularly spaced in range and bearing depends on the type of surface. The sum of these returns is called "reverberation" in sonar. If we write the distance to each elementary surface as $r + \Delta r_i$ then the audible signal can be approximated by the form

$$s_a(t) = K' \frac{1}{\mathcal{J}} \alpha_r^i \sum_{i=1}^{n} H_{\theta,\lambda}^i R_{\lambda,\theta}^i \sigma_{r,\lambda}^i \mathrm{Re}\left\{e^{2\pi j \frac{2m}{c}(r+\Delta r_i)t_s}\right\} \quad (2)$$

where $K' = \frac{KA^2}{2}$ (K is the modulation factor), $\mathcal{J}$ is the product of the sensitivities of the T/R pair, α_r describes the attenuation of the signal in the air, $H_{\theta,\lambda}$ is the directivity factor of the T/R pair, $R_{\lambda,\theta}$ is the reflectivity coefficient, $\sigma_{r,\lambda}$ represents the spreading of the reflection, and n is the number of returns. The signal consists of a narrow band of tones representing each reflecting point on the total surface, forming a spectrum of signals uniquely related to the geometry of the object in space and consequently having a unique audible character.

The amplitude of $s_a(t)$ will vary in a theoretically predictable manner if the reflection surface can be modeled, but in practice this is very difficult for complex objects.

3 Reflections from planes, corners, and edges

In the last section a very general description of the system's operation was presented. Let us now concentrate on cases of reflections from well structured objects like planes, corners, and edges.

3.1 Planes

Assume that we have a pair of pistons, displaced by b (0.01m), of diameter a (0.01m) (figure 2) mounted on a base able to rotate in one direction. The pressure at a field point can be obtained by dividing the surface of the piston into infinitesimal elements, each of which

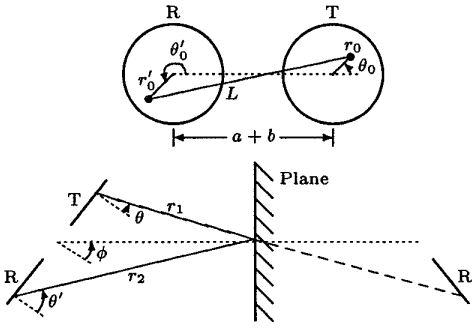

Figure 2: The T/R pair and a reflection from a plane.

acts like a baffled simple source of strength $dQ = Q_0 dS$ (assume that the piston vibrate in the perpendicular direction with speed $Q_0 \exp(j\omega t)$). The position r_0 of each of these elementary sources can be given in terms of polar coordinates r_0, θ_0, where θ_0 is the angle measured from the vertical axis in the piston plane. It is supposed that the reflectivity of the plane is 1, and there is no spreading of the signal on each reflection. Then, the receiver can be considered as its mirror image on the plane. The pressure at distance r generated by one of these sources is given by [6]

$$dp(r,t) = j\rho c \frac{Q_0 k}{2\pi r} e^{j(\omega t - kr)} dS \quad (3)$$

where $dS = r_0 dr_0 d\theta_0$ and $k = \frac{2\pi}{\lambda}$ (λ is the wavelength). The signal transmitted $s_T(t)$ is related to the pressure level by $\frac{ds_T(t)}{|dp(1,t)|} = \mathcal{J}_T$, where $\mathcal{J}_T$ is the sensitivity of the transmitter, and $dp(1,t)$ is the pressure level from a simple pair of T/R at 1m distance. In a similar manner, the signal received, $s_R(t)$ $\frac{ds_R(t)}{|dp_R|} = \mathcal{J}_R$, where $\mathcal{J}_R$ is the sensitivity of the receiver, and dp_R is the pressure level at the corresponding element of the receiver. By integrating over the surface of the transmitter S and the receiver S', we get

$$s_R(t) = \left| j \frac{s_T(t-\tau)}{\mathcal{J}_T \mathcal{J}_R} \int_S \int_{S'} \frac{e^{j(\omega(t-\tau)-kr)}}{r} dS dS' \right| \quad (4)$$

since $|p(1,t)| = \frac{1}{2\pi}\rho_0 c Q_0 k$. The distance r ($r_1 + r_2$) is given by the relationships $r' = r - r_0 \cos\theta_0 \sin\theta$ and $R = r' - r_0' \cos\theta_0' \sin\theta'$, where R is the distance between the centers of the T/R pair, r' is the distance between the center of the transmitter and dS', and θ and θ' the angles of incidence at the transmitter and the receiver. Equation 4 can be rewritten as

$$s_R(t) = \left| j \frac{s_T(t-\tau)}{\mathcal{J}_T \mathcal{J}_R} \frac{e^{j(\omega(t-\tau)-kR)}}{R} \right| \cdot \left| \int_S \int_{S'} e^{jk(r_0 \cos\theta_0 \sin\theta + r_0' \cos\theta_0' \sin\theta')} dS dS' \right| \quad (5)$$

where θ and θ' are related to the angle between the transducer and reflector plane ϕ (when $\phi \neq 0$) by

$$\sin\phi = \frac{2L + r(\sin\theta - \sin\theta')}{L(\sin\theta + \sin\theta')} \cdot \cos\left(\frac{\phi}{|\phi|} max\{|\theta|, |\theta'|\} - \phi\right)$$

$$\frac{r\sin\theta' - L}{\sin\theta + \sin\theta'} = \frac{r\cos\theta'}{\cos\theta + \cos\theta'} \quad (6)$$

L is the distance between the two sources on the transducer plane, $L^2 = (a+b)^2 + r_0^2 + (r_0')^2 + 2r_0 r_0' \sin(\theta_0 + \theta_0') + 2(a+b)(r_0\cos\theta_0 + r_0'\sin\theta_0')$.

By relating equations 3 and 5, it is obvious that the magnitude of the double integral of this equation corresponds to the directivity factor $H_{\theta,\lambda}$ of the pair T/R . The attenuation α_R of the signal is approximated by $1/R$ (this is true theoretically for the simple ray based model above; in practice there is likely to be more spreading). To simplify the calculations involved in equation 5, it is assumed that the difference between θ and θ' is due to the displacement $a+b$, which means that they are constant for every dS and dS' so that $L = a+b$ and $r = R$ in equations 6. Then $H_{\theta,\lambda} = N(\theta,\lambda)N(\theta',\lambda)$, where $N(\theta,\lambda) = \frac{2\pi a J_1(ka\sin\theta)}{ka\sin\theta}$.

The minimum area of the plane in order for the reflectivity to be 1 has to be a circle of diameter $a\cos\phi$. In smaller plane reflectors, the reflectivity will be dependent on their size and λ.

The radiation patterns produced by a piston-type T/R pair differ to some extent from these discussed previously. The reasons for this discrepancy is that the area of the baffle in which the transmitter is mounted is finite, the radiation from the back of the transmitter may propagate into the region in front of it, so that the resulting radiation pattern approximates that of an acoustic doublet rather than that of a piston in an infinite baffle, and the material of an actual transmitter cone is not perfectly rigid, [7].

3.1.1 Corners

Corners of perpendicular planes have exactly the same characteristics as planes, but the angles of incidence at the transmitter and receiver are given by $\theta = -\theta' = \phi$. In this case $H_{\theta,\lambda} = N(\theta,\lambda)^2$.

The maximum length for each side of the corner to get full reflection is given by $N_1 = \frac{2a+b}{2}\frac{\cos\phi}{\cos\phi'}$ and $N_2 = \frac{2a+b}{2}\frac{\cos\phi}{\sin\phi'}$ where ϕ' is the angle between one of the planes of the corner and the line which connects the transducer with the corner.

3.1.2 Edges

In this case, due to the spreading of every transmitted ray, all the elementary receivers will receive a fraction of the signal. So the signal at the receiver due to transmission from a simple source will be

$$ds_R(t) = \left| j\frac{ds_T(t-\tau)}{\mathcal{J}_T\mathcal{J}_R}\int_{S'}\frac{e^{j(\omega(t-\tau)-kr)}}{r}\sigma_{r,\lambda}dS'\right| dS \quad (7)$$

where $\sigma_{r,\lambda} = \frac{1}{2\pi\sqrt{r_2/\lambda}}$ and r_2 is the distance of each receiving element from the spreading point on the edge for each transmitted ray, $r_2 = r\frac{\cos\theta}{\cos\theta+\cos\theta'}$. Because r_2 affects only amplitude and $\theta - \theta'$ is small over the region of interest, we approximate it as $R/2$. Then $H_{\theta,\lambda}$ takes same form as for planes, but $s_R(t)$ depends on $\sigma_{r,\lambda}$ as well.

3.1.3 The CTFM sonar image

We have now defined all the parameters of the model for the cases of plane, corner and edge reflectors. The beat signal is given by

$$s_a(t) = F\alpha_R H_{\theta,\lambda}\sigma_{R,\lambda} Re\left\{e^{2\pi j\frac{m}{c}Rt_s}\right\} \quad (8)$$

which corresponds to a sinusoid of frequency proportional to the range but with constantly changing amplitude, due to the dependence of $H_{\theta,\lambda}$ and $\sigma_{R,\lambda}$ on λ. F is a factor dependent on the sensitivities $\mathcal{J}_T$, $\mathcal{J}_R$, on A, and on K. The CTFM sonar image is the Fourier transform of the beat signal

$$S_a(f) = \frac{1}{2}F\alpha_R\left(X(f - \frac{mR}{c}) + X(f + \frac{mR}{c})\right) \quad (9)$$

where $X(f)$ is the Fourier transform of $H_{\theta,\lambda}\sigma_{R,\lambda}$. Both $H_{\theta,\lambda}$ and $\sigma_{R,\lambda}$ are dependent on λ which is a function of t. This affects the calculation of $X(f)$, which is dependent on the angle ϕ, the range R and λ. So the image consists of a cosine modulated by the directivity and spreading signals, which are varying with time and angle ϕ and affect the amplitude and shape of the tone.

3.2 Discrimination between planes, corners, and edges

It is of interest to examine the variations of peak amplitude with respect to the orientation of the sensor. In figure 3, the change of the tone amplitude with respect to the orientation of the sensor is presented for the case of a plane, a corner, and an edge using the previous expressions (dashed lines), together with the equivalent experimental results (solid lines). The theoretical results match very well with the experimental for corners and edges but they differ slightly for planes. This is due to the simplifications made in equations 6, because the difference between θ and θ' increases with the width of the amplitude envelope and to saturation effects at the receiving system. The planes have a larger beam width (defined as the region over which

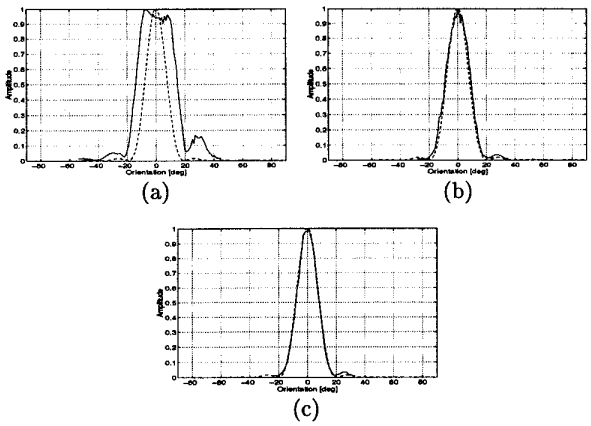

Figure 3: Variation in amplitude with the orientation for a plane (a), a corner (b), and an edge (c). The maximum amplitude is normalized to 1 in each plot.

the amplitude is within 3dB of the peak), and a high maximum amplitude. The corners in practice have a narrower beam width but also a high maximum amplitude. Finally, the edges too have a narrow beam width but a low amplitude, because of the spreading coefficient.

A set of two features is sufficient to describe these differences between the three types of reflectors. One is the beam width of the amplitude envelope (F_1), and the other the maximum amplitude (scaled with the attenuation factor α_r) (F_2). In order to test how effective the discrimination of the reflectors can be, the set of these features was derived for three cases for each reflector type (table 1).

	Planes		Corners		Edges	
	min	max	min	max	min	max
F_1	23	32	14	16	11	12
F_2	752	1316	668	1326	268	306

Table 1: The features values which discriminate planes, corners, and edges.

4 Detection of simple tonal reflectors

We will describe patterns corresponding primarily to a single tone, such as the ones above, as resulting from simple tonal reflectors. The detection of simple tonal from complex reflectors is essential in room mapping problems. In order to discriminate between these two distinct classes a tone indicator is sought which will describe the extent to which a given pattern has the shape of a tone, i.e. a single peak.

The region of the image which includes the pattern is isolated by filtering and transferred to the baseband [8]. Then a TLS-Prony model of nth order is used to estimate this region [9]. The frequencies of the n poles correspond to the peaks' ranges and their amplitudes to the peaks' values. In the case of a simple tonal pattern all the peaks with high amplitudes should appear in very close range. In contrary, in a complex pattern the high amplitude peaks are distributed in all over the selected region. A feature which points out these differences is given by

$$F = \sum_{i=1}^{n} \{((f_i - f_0)^2 p_i)^2 threshold(p_i)\} \qquad (10)$$

where f_i and p_i are the location and normalized amplitude of the ith pole and f_0 is the location of the highest amplitude pole and $threshold(p_i)$ is a function whose value is 1 if p_i is above a threshold level of amplitude, and 0 if it is below. By this way we include only the poles of high amplitude in the calculations of the tone indicator. An example of how this method works is illustrated in figure 4 for a plane and a curtain (n=50).

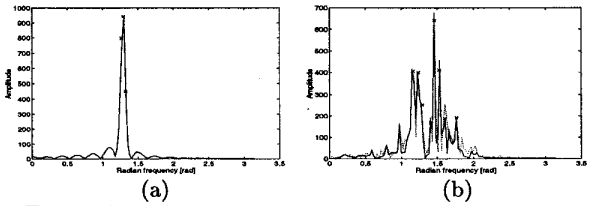

Figure 4: The poles locations of two selected regions.

The efficiency of this feature is tested on a set of typical reflectors in an indoor environment (three planes, three corners, three edges, and three reflections from a curtain). Table 2 presents the corresponding values of F. As it is observed there are significant differences in the values between tonal and complex reflectors which can easily be distinguished by applying a thresholding operation.

	Tonal patterns		Complex patterns	
	min	max	min	max
F	0.076	0.961	1483.854	3651.623

Table 2: The F values for simple and complex patterns.

5 A room mapping problem

Finally we illustrate the use of these methods to map a simple room. It is bounded by six walls which include a curtain, a wall light and a door with its frame. We aim to provide a spatial map of this room and to extract all possible information for each reflector type. A very simple and computationally cheap way to detect and locate the reflectors at the borders of the room

is based on the fact that the greatest return from a surface occurs when it is normal to the transmitted beam. We proceed as follows.

1. Determine the position of clusters through identifying the points of maximum amplitude in the scan image at each orientation.

2. Isolate any simple tonal reflectors from the scan image at each orientation.

3. Locate the range of the point of maximum amplitude of the reflector. This allows us to determine orientation.

4. Reconstruct a Cartesian image of the boundary of the room through integration of results from adjacent tonal reflectors.

5.1 Experimental results

To start with, a full scan of the room in a horizontal direction was taken with 1° step in the azimuth angle. Then a two dimensional matrix (called scan image, figure 5) was constructed by these measurements, where each column corresponds to the sonar image at each orientation. It can be seen that each reflector will appear as a cluster in the scan image. The width in the orientation axis of each cluster is due to the wide angular beam of the sensor, while the width in the range axis is due to the complexity of the reflector.

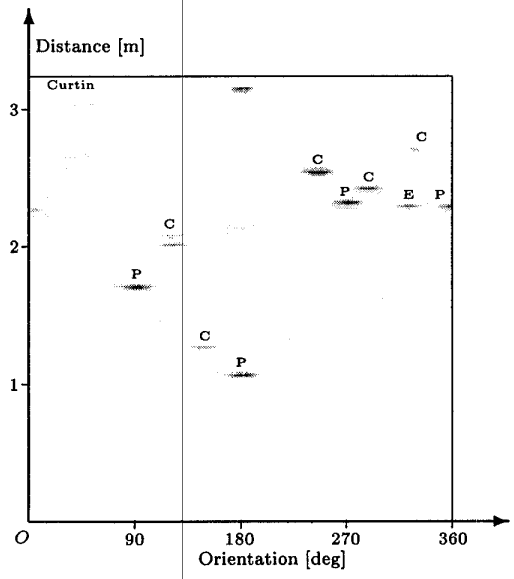

Figure 5: The resulting scan image (for clarity the figure only includes points above a certain threshold and the amplitude of each cluster is normalized). Notations P, C, and E correspond to planes, corners, and edges respectively.

5.2 Detection of reflectors

The locations of the detected reflectors in the room map are illustrated in figure 6 (points 1 to 14). These mark the position of maximum amplitude in each orientation. Increasing the step size up to 10° won't affect the detection of the targets, but the accuracy of the bearing estimation will be much lower. To use such a sparse scan we have to retain all the clusters appearing in the scan image by extracting not just the maximum point of the CTFM sonar image at each orientation, but all points corresponding to the major peaks.

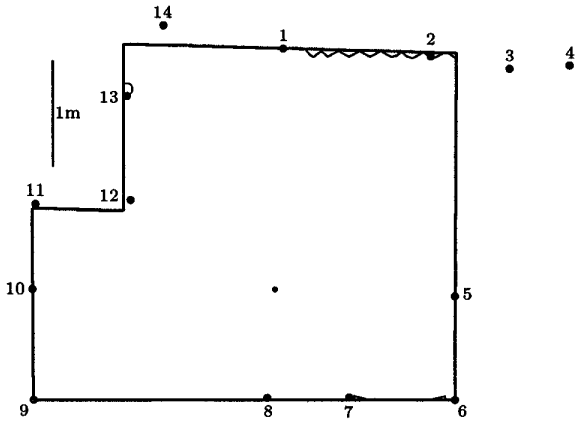

Figure 6: The room borders.

5.3 Isolation of simple tonal reflectors

Once the position of clusters is determined, the tone indicator is used to distinguish simple from complex tonal clusters. We see this in the real data. Points 2,3,4 and 6 were classified as complex reflections. 2, 3, and 4 correspond to the curtain. Point 6 corresponds to a corner, but where the frame of the door affects the image pattern so that it consists of multiple peaks.

5.4 Discrimination between planes, corners, and edges

The simple tonal reflectors were classified using the method of section 3. Three points (out of fourteen) were classified in error. It is likely that the errors occurred owing to the simplicity of the model; in particular because of inaccurate estimation of the function (α_r) which describes the dependence of image amplitude on the distance. We then determine the orientation of each structured reflector by examining the change in amplitude with orientation. The maximum amplitude does not always correspond to the true orientation; the middle point of the distribution is often a better estimator. Using these angles a new map of the room is obtained, presented in figure 7. Note that second order reflections 3 and 4 can be excluded using this method, because they appear on the other side of an identified plane (5) and at ranges where the curtain

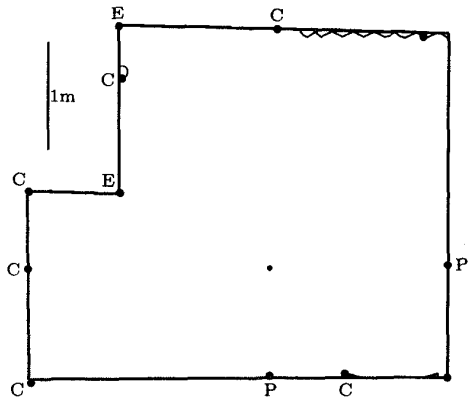

Figure 7: The located and identified borders.

image should be located. In addition reflections 3 and 4 have similar pattern with 2.

5.5 Integration of features

Given a knowledge of the basic geometry of the room, integration of the results can be used to improve accuracy. Assume three successive reflector positions. If the middle point is a plane, then all of them should be lying at the same line. If it is a corner, then the two outer points should be closer to the sensor. And finally, if the reflector is an edge, the two points should be further from the sensor.

Planes and corners have one tonal indicator in common, as do corners and edges. Therefore errors between these two groups of features are more likely than between planes and edges, and the initial estimate is overridden in these two groups if the class of reflector does not agree. However we do not reclassify planes as edges or vice versa. In addition we check the orientation of features, to see if a collinear assumption is justified.

By applying all these simple rules, the map of figure 7 will be changed. Reflectors 1 and 10 become planes. Reflector 13 is classified as an unknown object, because the feature values of F_1 and F_2 suggest a corner but the orientation does not line up with adjacent features (in fact it is caused by an object protruding from the wall). The same thing is valid for reflector 7. Finally, reflector 14 is confirmed as a corner.

6 Conclusions

In this paper we have seen that a set of different features appearing in the CTFM sonar image can provide sufficient information to discriminate between different types of reflectors. Such feature recognition is based on geometrical modeling (unrelated to the transmitted signal pattern), hence it is not unique to the CTFM sonar. However, the increased energy available from the continuous wave radiation provides clearer information through the improved signal to noise ratio.

Early results of using this system have confirmed the advantages and demonstrated a simple method for map building. The algorithms exploit both range and amplitude information and the wide beam of the sonar potentially enables it to track objects in different orientations using a single image. The main difficulty lies on the robustness of target's identification, caused by the over simplistic representation of amplitude's dependence on distance (further experiments suggest that the air absorption should be considered), and the saturation effects produced by the highly powered transmitted signal. At the present methods to eliminate these effects are investigated.

Acknowledgements

We have to thank Steve Reece for his suggestions. One author, Z. Politis, is supported by the State Scholarships Foundation (SSF) of Greece.

References

[1] J. Leonard and H. Durrant-Whyte. Mobile robot localization by tracking geometric beacons. *IEEE Transactions on Robotics and Automation*, 7(3):376–382, June 1991.

[2] B. Barshan and R. Kuc. Differentiating sonar reflections from corners and planes by employing an intelligent sensor. *IEEE Transactions on Pattern Analysis and Machine Intelligence*, 12(6):560–569, June 1990.

[3] H. Peremans K. Audenaert and J. M. Van Campenhout. A high-resolution sensor based on tri-aural perception. *IEEE Transactions on Robotics and Automation*, 9(1):36–48, February 1993.

[4] L. Kay. A sonar aid to enhance spatial perception of the blind: Engineering design and evaluation. *The Radio and Electronic Engineer*, 44(11):1974, November 1974.

[5] L. Kay and M. A. Do. An artificially generated multiple object audiotory space for use where vision is impaired. *Acustica*, 36(1):1–8, 1976/77.

[6] L. E. Kinsler A. R. Frey A. B. Coppens and J. V. Sanders. *Fundamentals of Acoustics*. John Wiley & Sons, third edition, 1982.

[7] P. M. Morse and K. Uno Ingard. *Theoretical acoustics*. Princeton University Press, 1968.

[8] Z. Politis. *Perception of a Robot Workspace by Extracting Navigational Information Using CTFM Sonar Imaging*. Transfer report, University of Oxford, Trinity Term 1997.

[9] W. M. Steedly C. J. Ying and R. L. Moses. Statistical analysis of TLS-Based prony techniques. *Automatica*, 30(1):115–129, 1994.